Environ. Sci. Technol. **2004**, *38,* 5078−5086

Interaction of Uranyl with Calcite in the Presence of EDTA

SOPHIE RIHS,† NEIL C. STURCHIO,* KENT ORLANDINI, LIKWAN CHENG, HENRY TENG,‡ PAUL FENTER, AND MICHAEL J. BEDZYK§

Argonne National Laboratory, 9700 South Cass Avenue, Argonne, Illinois 60439-4843

Adsorption of uranyl at the surface of calcite was investigated by using batch sorption experiments and synchrotron X-ray standing wave (XSW) measurements. Aqueous solutions containing ^{236}U(VI) (4.5×10^{-7} to 1.0×10^{-4} M) and EDTA (5.0×10^{-7} to 1.1×10^{-4} M) were reacted for 90 s to 60 min with freshly cleaved calcite (104) surfaces and calcite powders. Surface exchange coefficients, sorption kinetics, and influence of powder surface area/solution volume (SA/V) ratio were investigated by α-counting of ^{236}U. Powder sorption results at SA/V = 870 cm^2/mL fit a Freundlich isotherm [log $[U]_{surface}$ (in monolayers) = log K + n log $[U]_{aq}$ (in moles/L)], where K = 1.9 ± 0.5 and n = 0.9 ± 0.1, consistent with uptake of U(VI) by a specific surface reaction where the availability of sorption sites is nonlimiting in the U concentration range measured. Measured U(VI) coverages along this isotherm, based on the calcite (104) surface Ca site density, ranged from 0.04% to 5.4% of a monolayer. Steady state surface coverages were obtained within 90 s. Sorption of U(VI) on calcite (104) single-crystal cleavage surfaces using identical solutions yielded higher coverages, because of increased step density induced by dissolution at the relatively low SA/V ratio (∼1) of these measurements. The crystallographic location of the sorbed U(VI) was examined with the synchrotron XSW technique. Measurements were performed at the Advanced Photon Source on fresh calcite (104) cleavage surfaces reacted for 90 s with U(VI) solutions. Coherent fractions for sorbed U ranged from 0.14 to 0.62, and the mean value of the U coherent position was 0.84 ± 0.02. This position was independent of dissolved U(VI) concentration and corresponds to a distance between the U atom and the calcite (104) plane of 2.55 ± 0.06 Å. These results are consistent with U(VI) adsorption at the calcite surface as an inner-sphere uranyl−carbonate surface complex bonded with the outer oxygen atom(s) of a single surface carbonate group. Steric considerations allow this observed U(VI) surface complex to occur both at step sites ($\langle\bar{4}41\rangle$_ and $\langle 48\bar{1}\rangle$_) and on terrace areas adjacent to Ca vacancies.

* Corresponding author phone: (312)355-1182; fax: (312)413-2279; e-mail: Sturchio@uic.edu. Present address: Department of Earth and Environmental Sciences, University of Illinois at Chicago (MC-186), 845 West Taylor Street, Room 2476, Chicago, IL 60607-7059.

† Present address: Centre de Géochimie de la Surface, Université Louis Pasteur (UMR 7517), 1 rue Blessig, 67084 Strasbourg Cedex, France.

‡ Present address: Department of Earth and Environmental Sciences, The George Washington University, 2029 G. St. NW, Washington, DC 20052.

§ Present address: Department of Materials Science and Engineering, Northwestern University, Evanston, IL 60208.

Introduction

Characterization of radionuclide mobility in the environment is a major goal of applied geochemistry. Uranium(VI) mobility in oxic surface waters and groundwaters is strongly enhanced by the formation of stable uranyl−carbonate complexes (*1*, *2*). The formation of these uranyl−carbonate complexes is controlled by pH and CO_2 partial pressure, and in most bicarbonate groundwaters the dominant species of U(VI) are uranyl−carbonate anions. Experimental studies of U(VI) adsorption have been performed with various solids including quartz, α-alumina, clinoptilolite, amorphous silica, hydrous Fe-oxides, clays, and gels (*3*−*22*). Froideval et al. (*22*) reviewed literature about U(VI) surface complexation. In most cases, U(VI) sorption involves mononuclear bidentate surface compexation. However, Chisholm-Brause et al. (*19*) and Sylwester et al. (*18*) showed that outer-sphere U(VI) complexes may coexist in some cases. The pH dependence of U(VI) sorption on these materials is generally similar, suggesting that U(VI) sorption is not as sensitive to the surface charge characteristics of the sorbent as it is to the effective surface area (*13*). Among these minerals, Fe-oxides are believed to be of particular importance, due to their high sorptive capacities for U (*6*, *8*). However, several studies show that the complexation of uranium with dissolved carbonate significantly decreases U(VI) adsorption onto Fe-oxides (*4*, *8*, *9*, *11*, *16*, *17*). In natural CO_2-rich groundwater systems, it has been shown that up to 90% of the initial U(VI) can remain in the water, despite the precipitation of iron hydroxides and calcite (*23*). Predictions of U(VI) interaction with mineral surfaces are complicated by the fact that U(VI) does not exist as a free metal ion in aqueous environments but develops strong covalent bonds with two oxygen atoms, forming the linear uranyl moiety UO_2^{2+}.

Few studies have addressed the sorptive and coprecipitative behavior of U(VI) with respect to carbonate minerals (*24*−*30*). Calcite is a ubiquitous component of sediments both in freshwater and marine environments, in which uranium can be efficiently trapped over at least several hundreds of thousands of years as evidenced by U-series age determinations (*31*). Most previous studies of the interaction of uranium with calcite involved macroscopic measurements on powder experiments, generating useful information about thermodynamic parameters. However, a comprehensive atomic-scale view of the U(VI) binding mechanism with the calcite surface is still lacking. Because of advances in analytical methods, in-situ synchrotron techniques are now suitable for this purpose. For instance, recent work of R. J. Reeder and colleagues (*28*−*30*) addressed mechanisms of U(VI) uptake by coprecipitation with and adsorption to calcite, using X-ray absorption fine structure (XAFS) and luminescence spectroscopy. Geipel et al. (*32*) used XAFS and time-resolved laser induction fluorescence spectroscopy to investigate the interaction of uranyl solutions with calcite. Sturchio et al. (*33*) used XAFS and X-ray fluorescence microprobe to demonstrate that tetravalent U substitutes for Ca in a 35 million-year-old calcite, and Kelly et al. (*34*) used the same techniques to show that hexavalent U substitutes for Ca in a late Pleistocene calcite.

We investigated U(VI) sorption onto the calcite (104) cleavage surface using batch sorption experiments, α-spec-

10.1021/es049847b CCC: $27.50
Published on Web 09/02/2004

TABLE 1. Formation Constants[c] of U(VI) Species Used in the Calculation of the Uranyl Speciation

reaction	Log β°	ref
$UO_2^{2+} + H_2O \leftrightarrow UO_2OH^+ + H^+$	−5.2	(*2*)
$UO_2^{2+} + 2H_2O \leftrightarrow UO_2(OH)_2^0 + 2H^+$	−11.5	(*43*)
$UO_2^{2+} + 3H_2O \leftrightarrow UO_2(OH)_3^- + 3H^+$	−19.74	(*44*)
$UO_2^{2+} + 4H_2O \leftrightarrow UO_2(OH)_4^{2-} + 4H^+$	−33	(*2*)
$2UO_2^{2+} + 2H_2O \leftrightarrow (UO_2)_2(OH)_2^{2+} + 2H^+$	−5.62	(*2*)
$2UO_2^{2+} + H_2O \leftrightarrow (UO_2)_2OH^{3+} + H^+$	−2.7	(*2*)
$3UO_2^{2+} + 5H_2O \leftrightarrow (UO_2)_3(OH)_5^+ + 5H^+$	−15.55	(*2*)
$3UO_2^{2+} + 4H_2O \leftrightarrow (UO_2)_3(OH)_4^{2+} + 4H^+$	−11.9	(*2*)
$3UO_2^{2+} + 7H_2O \leftrightarrow (UO_2)_3(OH)_7^- + 7H^+$	−31.0	(*2*)
$4UO_2^{2+} + 7H_2O \leftrightarrow (UO_2)_4(OH)_7^+ + 7H^+$	−21.9	(*2*)
$UO_2^{2+} + HEDTA^{3-} \leftrightarrow UO_2HEDTA^-$	7.4[a]	(*45*)
$2UO_2^{2+} + EDTA^{4-} \leftrightarrow (UO_2)_2EDTA^0$	17.87[a]	(*45*)
$2UO_2^{2+} + 2EDTA^{4-} \leftrightarrow (UO_2)_2(EDTA)_2^{4-}$	26.77[b]	(*45*)
$2UO_2^{2+} + EDTA^{4-} + H_2O \leftrightarrow (UO_2)_2(OH)(EDTA)^- + H^+$	13.06[b]	(*45*)
$4UO_2^{2+} + 2EDTA^{4-} + 4H_2O \leftrightarrow (UO_2)_4(OH)_4(EDTA)_2^{4-} + 4H^+$	15.34[b]	(*45*)
$6UO_2^{2+} + 3EDTA^{4-} + 4H_2O \leftrightarrow (UO_2)_6(OH)_4(EDTA)_3^{4-} + 4H^+$	34.3[b]	(*45*)
$UO_2^{2+} + NO_3^- \leftrightarrow UO_2NO_3^+$	0.29	(*2*)
$UO_2^{2+} + CO_3^{2-} \leftrightarrow UO_2CO_3^0$	9.68	(*2*)
$UO_2^{2+} + 2CO_3^{2-} \leftrightarrow UO_2(CO_3)_2^{2-}$	16.94	(*2*)
$UO_2^{2+} + 3CO_3^{2-} \leftrightarrow UO_2(CO_3)_3^{4-}$	21.60	(*2*)
$UO_2^{2+} + 3CO_3^{2-} + Ca^{2+} \leftrightarrow UO_2(CO_3)_3Ca^{2-}$	25.4[f]	(*46*)
$UO_2^{2+} + 3CO_3^{2-} + 2Ca^{2+} \leftrightarrow UO_2(CO_3)_3Ca_2^0$	30.55[f]	(46)

[a] $I = 0.1$ M. [b] $I = 1$ M. [c] At 25 °C and $I = 0$, except where specified otherwise.

trometry, and synchrotron X-ray standing wave (XSW) measurements. The objective of these experiments was to define the mode of sorption as well as to constrain the molecular structure of uranyl species on calcite in the presence of ethylenediaminetetraacetic acid (EDTA). This organic chelating ligand is a common constituent of liquid nuclear waste streams (*35*−*37*), e.g. in the vicinity of high-level nuclear waste storage tanks near Richland, Washington (*38*), and U released to the environment with such waste may thus be associated with EDTA and other organic complexants. In addition, EDTA is also a widespread contaminant of surface water and groundwater because of its common use in industry and agriculture (*39*). The interaction of U(VI) with organic complexants, whether synthetic or naturally occurring, may significantly influence U transport behavior in the environment (*40, 41*).

Experimental Section

Sorption Experiments. Batch sorption experiments were conducted at room temperature (23 ± 1 °C). Various U(VI) solutions were reacted with two sorbents: (1) reagent calcite powder and (2) freshly cleaved crystals of natural spar calcite.

Solutions. Uranium(VI) stock solution was obtained by dissolution of a ^{236}U nitrate salt [$UO_2(NO_3)_2 \cdot 6H_2O$] in a Na_2EDTA aqueous solution to yield a solution of 1.0×10^{-4} M U and 1.1×10^{-4} M EDTA. The presence of EDTA ensures undersaturation with U(VI) solid phases. Experimental solutions of lower concentration were prepared by dilution of the stock solution with deionized water. No additional background electrolyte or pH buffer was used. The ionic strength in all solutions was lower than 0.001 M.

Calculation of aqueous U speciation was performed using the MINTEQA2 3.11 code (*42*). Thermodynamic data for aqueous uranyl species were supplemented or replaced with those listed in Table 1. Constants of EDTA deprotonation and Ca−EDTA complexation were taken from ref *45*. Solubility constants of U-bearing solid phases were adjusted to be consistent with the NEA database (*2*). The solubility constant of "amorphous" schoepite from ref *47* was also added to the database. Activity coefficients were calculated using the Davies equation.

Calculations of U speciation in the initial solutions, assuming atmospheric P_{CO_2}, show that 32% to 84% of U was complexed with EDTA, the remainder being uranyl−hydroxyl or uranyl−carbonate complexes and uranyl ions. All the U-bearing solid phases in the database of MINTEQA2, including schoepite ($(UO_2)_8O_2(OH)_{12} \cdot 12(H_2O)$), amorphous schoepite, β-$UO_2(OH)_2$, and rutherfordine (UO_2CO_3), were undersaturated in these solutions. Saturation indices of these phases ranged from −0.4 to −4.5, from −1.3 to −5.6, from −0.5 to −4.8, and from −2.8 to −9.7, respectively. For some of these U(VI) solutions, similar pH and P_{CO_2} conditions in the absence of dissolved EDTA would have caused schoepite saturation (SI ≈ 0 instead of −0.4).

Sorption on Calcite Powder. Reagent $CaCO_3$ powder (Merck) was prepared by stirring it magnetically in deionized water (pH ∼ 6) for several days and then rinsing and decanting it several times with fresh deionized water to remove smaller particles. The powder was then dried at 110 °C and stored in a closed container. The initial surface area of the calcite powder (after outgassing at 100 °C for 16 h) was 0.87 m^2/g as determined from an eight-point N_2−B.E.T adsorption isotherm, by using an automated Quantachrome Corp. Autosorb-6 analyzer.

Batch experiments on the prepared calcite powder were conducted by reacting, in polypropylene centrifuge tubes, about 0.5 g of powder with various volumes of U(VI) solutions (so that the solid mass to solution volume ratio ranged from 0.025 to 0.2 g/mL) in which U(VI) initial concentrations ranged from 4.5×10^{-7} to 1.0×10^{-4} M. The centrifuge tubes were loosely capped, and the mixtures were stirred using a gyratory shaker. Reaction times ranged from 90 s to 60 min. Within the desired reaction time, the samples were centrifuged; the supernatant solution was then withdrawn, and the calcite powder was rinsed twice with 10−20 mL of methanol to eliminate any residual solution trapped within the powder.

We verified that rinsing with methanol removes residual solution from calcite powder without desorbing the U(VI) species. Aliquots of the same powder subjected to multiple rinses with methanol (accomplished by shaking the methanol−calcite mixture, then centrifuging it briefly, and pouring off the methanol supernate) showed that no change of the amount of ^{236}U in the powder occurred after two rinses. A separate test was performed with a ^{137}Cs solution (adjusted to pH∼8 with NH_4OH), using the same procedure and the

same calcite powder. In this range of pH, Cs is known to show negligible adsorption onto calcite (*48*), so any ^{137}Cs activity detected in the calcite powder would have implied trapping of interstital solution within the powder. The activity of ^{137}Cs in the initial and final solutions, in the reacted powder, and in the methanol rinse was directly measured by gamma spectrometry using a high efficiency coaxial HP−Ge detector. Results showed that a negligible amount of ^{137}Cs ($\ll$ 1%) was detected in the calcite powder, demonstrating the efficient removal of solution from the powder after two rinses with methanol.

The ^{236}U activity sorbed on the calcite powder was determined using isotope dilution α-spectrometry. The calcite powder was dissolved in nitric acid, spiked with a known activity of ^{238}U, and U was chemically purified using anion chromatography on AG1-X8 ion-exchange resin followed by electrodeposition of U onto polished stainless steel disks for alpha spectrometry. Each sample was counted for a time sufficient to achieve 1σ relative error of ±1.5% or better. The initial bulk concentration of U in the reagent calcite was 0.04 mg/kg; therefore, corrections to the ^{238}U spike activity used in determination of sorbed ^{236}U were negligible (<0.03%).

The pH of each experimental solution was measured before and after reaction by using an Orion pH meter with a combination electrode calibrated with NIST-traceable pH buffers. Initial pH values ranged from 4.4 to 5.8, and final pH values ranged from 10.3 to 10.7.

Sorption on Calcite Single Crystals. Sorption of U(VI) on calcite (104) cleavage surfaces was investigated. The calcite samples were cut from large, natural optical-quality Brazilian spar crystals and were cleaved immediately prior to reaction with ^{236}U(VI) solutions. Adsorption time was controlled by allowing several drops of the solution to react with the crystal surface for 90 s, after which the surface was rinsed with a jet of methanol. Activities of ^{236}U sorbed onto the crystal surfaces were determined by direct α-counting of the cleavage surfaces with an Al foil mask controlling the exposed surface area. For each solution ^{236}U(VI) concentration, two or three replicate crystals were measured. Because of the low calcite surface areas involved in the single-crystal experiments relative to the powders, a small number of ^{236}U atoms sorbed onto these samples, resulting in relatively large 1-σ counting errors (±10−20%). The bulk concentration of U in the calcite used for these experiments was 0.013 mg/kg.

Coverage Calculations. For the powder experiments, the measured surface area (S = 0.87 m^2/g) was used for the calculation of the U coverage, Θ_U, as given by

$$\Theta_U = \frac{[U]_s \times N}{S \times 5.04 \times 10^{14}} \quad (1)$$

where $[U]_s$ is the amount of sorbed U(VI) on the calcite (in moles per unit mass of powder), N is Avogadro's number (6.02×10^{23}), and 5.04×10^{14} is the number of Ca sites per cm^2 of the calcite (104) surface. For single crystals, in the absence of surface roughness measurements, we assumed a roughness factor of 1.2 to estimate the specific surface area (*49*) of our cleavage surfaces and thus the U(VI) coverage. This approximation may influence the comparison between single-crystal and powder sorption data but not the comparison between single-crystal results. Coverage is expressed in terms of monolayer fraction (where 1 monolayer = 5.04×10^{14} U atoms/cm^2).

X-ray Standing Wave (XSW) Techniques and Measurements. *Sample Preparation.* Five calcite (104) surfaces were cleaved and reacted with ^{236}U(VI) solutions for XSW measurements, following the same procedure as described above. Dissolved ^{236}U(VI) concentrations were 5.0×10^{-5}, 9.8×10^{-5}, and 1.3×10^{-4} mol/L. The crystals were positioned on a Kel-F sample cell inside a thin Kapton bag flushed with high-purity He gas for the duration of the XSW measurements. Measurements of U L-α fluorescence and Bragg reflectivity were made while scanning the sample angle through the calcite (104) Bragg reflection.

XSW Data Acquisition and Analysis. The X-ray standing wave technique, using Bragg reflections from bulk crystals, was reviewed recently (*50*). It has been applied to study trace elements in bulk calcite, at the calcite (104) surface, and at the rutile (110) surface (*51*−*58*). The fluorescent yield, $Y(\theta)$, from a specific element varies as a function of the angle θ according to the following equation

$$Y(\theta) = Y_{ob}[1 + R(\theta) + 2\sqrt{R(\theta)}f_{(hkl)}\cos(\nu(\theta) - 2\pi P_{(hkl)})] \quad (2)$$

where $R(\theta)$ is the reflectivity of the particular Bragg peak, Y_{ob} is the off-Bragg fluorescence, and $\nu(\theta)$ is the variation of the XSW phase as a function of the sample angle, θ. The coherent position, $P_{(hkl)}$, and the coherent fraction, $f_{(hkl)}$, of the fluorescent atom are two model-independent parameters representing the ion distribution and ranging in value from 0 to 1. The former corresponds to the $\Delta d/d$ fractional position relative to the (hkl) diffraction plane of the crystal lattice, whereas the latter measures the static and the dynamic spread of the atomic distribution. These two parameters are obtained from a χ^2 fit of eq 2 to the XSW data. Uncertainties in $P_{(hkl)}$ and $f_{(hkl)}$ are typically smaller than ±0.02 and are derived on the basis of counting statistics and a sensitivity analysis of the fitting procedure.

X-ray standing wave measurements of reacted calcite (104) cleavage surfaces were conducted at the undulator beamline 12-ID-D at the Advanced Photon Source during two separate runs in which the incident photon energies, selected by a double-bounce Si(111) monochromator, were 27.2 and 17.8 keV, respectively. The U−Lα fluorescence emission line at 13.6 keV was monitored using a Si(Li) solid-state detector with an energy resolution of ~250 eV, and the Bragg reflectivity was measured using an ion chamber. The fluorescence signal of the Sr−Kα line at 14.1 keV (from Sr in the bulk calcite) was minimized using detector slits to control the exit angle of the fluorescent radiation to increase the surface sensitivity and reduce spectral interference with U. The fluorescence signal from U was small, thus a large number of scans (between 200 and 800 scans, total duration of 3 to 13 h) were required to obtain good precision. While a number of measurements of U fluorescence modulation were made successfully at the (104) Bragg reflection, attempts using the (006) reflection were unsuccessful because of the much higher Sr fluorescence signal in that geometry.

AFM Images. Images of a representative calcite (104) cleavage surface before and after reaction with a dilute EDTA solution (with no added U) were obtained by tapping-mode atomic force microscopy (AFM) using a Digital Nanoscope IIIa Scanning Probe Microscope with a flow-through fluid cell. Images were recorded in deionized water and in 0.12 mM EDTA solution following a reaction time of 1 min. The most concentrated experimental solution used in our experiments was 0.11 mM EDTA; therefore, the AFM image collected after 1 min of reaction may represent the maximum effect of our experimental solutions on the calcite (104) surface. Using image-analysis software, we estimated that the total step density increased by about 80% after reaction with 0.12 mM EDTA.

Results

Batch Sorption Experiments. *Speciation of Dissolved U(VI).* The final pH values of the solutions were consistently around 10.5. This value is too high for a calcite solution in equilibrium

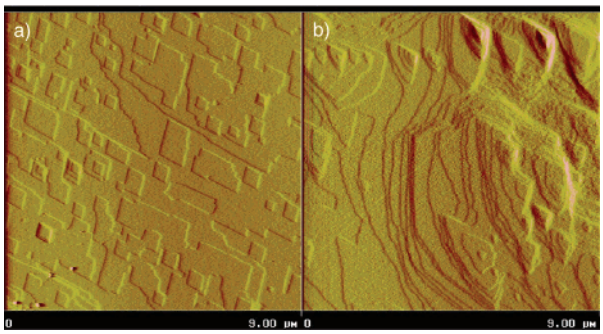

FIGURE 1. AFM images of the calcite (104) cleavage surface in contact with (a) deionized water and (b) after 1 min contact with 0.12 mM EDTA solution.

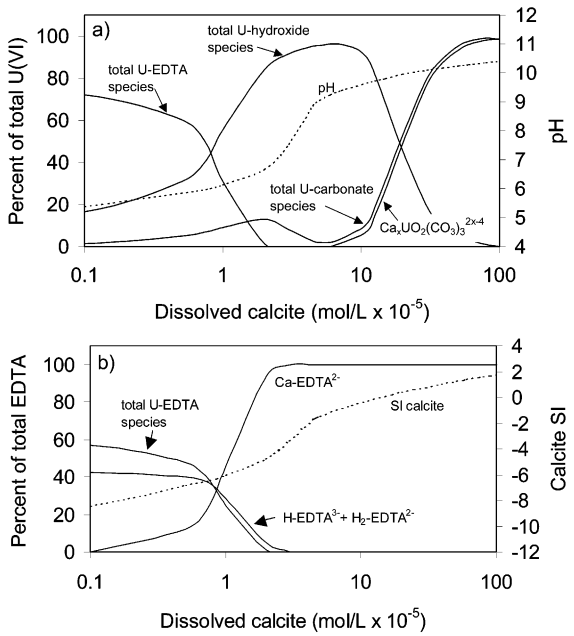

FIGURE 2. Predicted U speciation of experimental solutions as a function of the amount of calcite dissolved (individual species at pH < 6 left out for clarity): (a) U(VI) speciation (total U(VI) concentration = 4.5×10^{-6} M) where $Ca_xUO_2(CO_3)_3^{2x-4}$ represents the abundance of $Ca_2UO_2(CO_3)_3^0$ + $CaUO_2(CO_3)_3^{2-}$ species; (b) speciation of EDTA complexes (total EDTA concentration = 5.8×10^{-6} M) and saturation index (SI) of calcite.

with atmospheric CO_2, indicating that equilibration of solutions with atmospheric CO_2 was not achieved during the 90 s to 60 min durations of the experiments, perhaps because of the slow kinetics of the CO_2 conversion into HCO_3^- and H^+ (*59*) and the slow transfer of atmospheric CO_2 to solution. Reaction with the initial calcite-undersaturated EDTA-bearing U(VI) solutions caused dissolution of the calcite surface (Figure 1) along with pH increases and changes in U(VI) speciation.

A model of the change in speciation of one of the experimental solutions (4.5×10^{-6} M U(VI)), simulated with MINTEQA2 by adding Ca^{2+} and CO_3^{2-} in equimolar proportion to the initial solution until reaching pH 10.4, is shown in Figure 2a. As the pH increases from the initial value of 5.2 to about 5.9, the dominant U(VI) species are uranyl−EDTA species; between pH 5.9 and 9.9 the dominant U(VI) species are hydroxyl species; and above pH 9.6 the dominant U(VI) species are the uranyl−carbonate species $CaUO_2(CO_3)_3^{2-}$ and $Ca_2UO_2(CO_3)_3^0$. Calcite remains undersaturated until pH 10 is reached. Analogous calculations for the other experimental solutions produced similar end results. The total amount of calcite dissolved, based on these calculations, ranges from about 0.3 to 6.0 monolayers equivalent for the powder experiments.

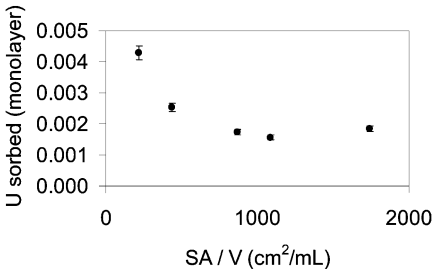

FIGURE 3. Influence of the SA/V ratio on U(VI) sorption on calcite powder. Reaction time = 90 s, U(VI) concentration in solution = 4.5×10^{-6} M.

Influence of Dissolved EDTA on the Calcite Dissolution Rate. The model used to simulate calcite dissolution also allows prediction of EDTA speciation. The evolution of the complexation of $EDTA^{4-}$ with Ca^{2+} ions liberated during calcite dissolution and the corresponding saturation index (SI) of the solution with respect to calcite are shown in Figure 2b. The model predicts that all dissolved EDTA was complexed with Ca^{2+} well before the end of the dissolution. Ca−EDTA complexes represent 100% of dissolved EDTA at the point when 3×10^{-5} mol/L of calcite has dissolved, whereas the model predicts that 100×10^{-5} mol/L of calcite must dissolve to reach the final measured pH = 10.4. At the point where all of the EDTA is complexed with Ca, the solution remains undersaturated with calcite.

EDTA has been shown to increase the rate of dissolution of calcite; surface complexation of EDTA with Ca ions of the mineral surface produces a weakening of the bonds between calcium and carbonate, resulting in desorption of the Ca−EDTA complex and the carbonate products (*60*). This mechanism is expected to proceed only when the EDTA is not completely saturated with Ca^{2+}. Moreover, Fredd and Fogler (*60*) show that at low EDTA concentration (i.e. 10^{-3} M), this chelation reaction is limited, and calcite dissolution is then governed by reactions with water. Friis et al. (*61*) observed a linear increase of calcite dissolution rate with EDTA concentration. This trend allows us to estimate that in 10^{-4} M EDTA (the highest concentration used in the present study), the expected calcite dissolution rate would be only about twice the rate in DI water.

Sorption Kinetics. Kinetics of U(VI) sorption were investigated by reacting aliquots of a U(VI) solution with aliquots of calcite powder (at a calcite surface area/solution volume ratio of 870 cm^2/mL) for times ranging from 90 s to 60 min. The measured U(VI) coverage did not change significantly during this time, suggesting that a steady state was attained within 90 s in our experimental system. Previous studies showed that the initial chemical sorption of heavy metals to mineral surfaces generally occurs on millisecond time-scales (*62*, *63*). This initial sorption is often followed by a slower period of sorption occurring on time scales of days and longer and generally attributed to interparticle diffusion in pores, sites of low reactivity, and surface precipitation (*64*−*67*). These long-term processes have been addressed elsewhere (*28*−*30*, *34*), and only the initial sorption step, remaining unclear, was investigated in the present study. How this initial step may be related to the subsequent incorporation of U(VI) in bulk calcite is discussed further below.

Surface Area/Volume Effect. The effect of the ratio of powder surface area to solution volume (SA/V ratio) on the amount of U(VI) sorption is shown in Figure 3. This set of experiments was performed with a constant initial U(VI) solution concentration of 4.5×10^{-6} M, but with varied amounts of solution reacting with 0.5 g aliquots of calcite powder for 90 s. The U(VI) coverage decreased from 0.0024

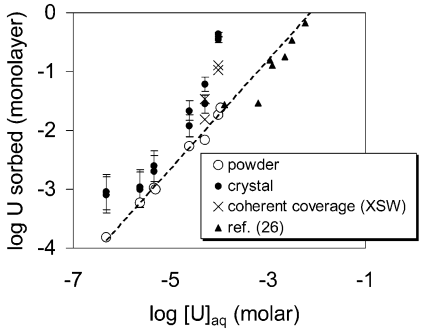

FIGURE 4. U(VI) sorption isotherm (in terms of U monolayers vs $[U]_{aq}$, M) on calcite powder and single crystals. Two or three replicates were performed for single crystals. Reaction time = 90 s for both powders and single crystals; SA/V ratio = 870 cm^2/mL for powders and ~1 for single crystals. Coherent coverage refers to single-crystal XSW experiments (see text for explanation). Also shown are results of ref *26*. Dashed line shows Freundlich isotherm calculated from powder results, which has the form log monolayers = log K + n log $[U]_{aq}$, where $K = -1.9 \pm 0.5$ and $n = 0.9 \pm 0.1$.

to 0.001 monolayers, as the SA/V ratio increased from 217 to 870 cm^2/mL. The coverage remained constant for higher SA/V ratios (1088 and 1740 cm^2/mL).

Sorption Isotherm. The U(VI) coverages on the surfaces of both calcite powder and single-crystal samples, as a function of the dissolved U(VI) concentration, are shown in Figure 4. The SA/V ratio for the powder experiments was 870 cm^2/mL, in the range where U(VI) coverage did not change with respect to SA/V ratio (Figure 3). U(VI) coverages on these samples ranged from 0.0001 to 0.025 monolayers, whereas dissolved U(VI) concentration varied from 4.2×10^{-7} to 9.4×10^{-5} M. These results are well fit by a Freundlich isotherm, using the following equation: $[U]_s = K \times [U]_{aq}^n$, where $[U]_s$ and $[U]_{aq}$ are the U(VI) concentration sorbed on calcite (monolayers) and U(VI) concentration (M) in the solution, respectively, and K and n are constants. Values of $n = 0.9 \pm 0.1$ and $K = 1.9 \pm 0.5$ were determined from our data (with a regression coefficient $R^2 = 0.9898$). These values predict that 1 monolayer coverage would be obtained at $[U]_{aq} = 7.7 \times 10^{-3}$ M. Similar Freundlich sorption behavior was observed for U(VI) sorption onto quartz (*13*) and montmorillonite (*20*).

Data from experiments performed with higher dissolved U(VI) concentrations by Carroll and Bruno (*26*) are also shown for comparison in Figure 4. These values were measured under atmospheric pCO_2 conditions, but with pH and SA/V ratios (pH = 7.2−7.5 and SA/V = 67 cm^2/mL) different from those in our experiments. No effect of the SA/V difference between the two sets of data is expected. Our calculated speciation of dissolved U(VI) showed predominance of uranyl−carbonate species for both studies. The similar trend between Carroll and Bruno's (*26*) data and our results confirms Freundlich isotherm behavior over a broad range in U(VI) concentration and demonstrates the pH independence of the U(VI) coverage within the stability range of the uranyl−carbonate complexes.

Sorption of U(VI) on calcite single crystals was consistently higher than that on calcite powder, with U(VI) coverages on the single crystals ranging from 0.0008 to 0.43 monolayer. One or more replicates were measured for each U(VI) solution concentration, showing good agreement in U(VI) coverage estimates of powders and single crystals for low dissolved U(VI) concentrations but significant discrepancies for samples reacted with 2.1×10^{-5} M and higher U(VI) solution concentrations. The higher coverage on the crystals may result from the relatively small SA/V ratio of the single-crystal experiments (~1 cm^2/mL) compared to that of the powder experiments (217 to 870 cm^2/mL). Experimental results for

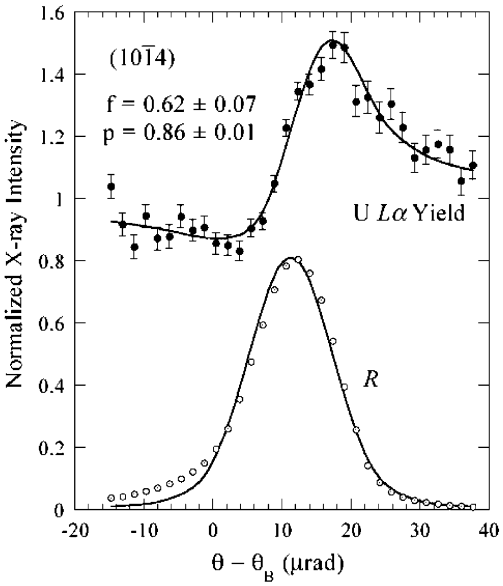

FIGURE 5. X-ray standing wave data for calcite (104) cleavage surface reacted with solution containing 5.0×10^{-5} M U(VI), showing angular dependence of the experimental U−Lα fluorescence yield *Y(θ)* (normalized to unity for off-Bragg angles, closed circles) and the X-ray reflectivity *R(θ)* of the calcite (104) reflection (open circles). Numerical best-fits to reflectivity (using dynamical diffraction theory) and fluorescence yield are shown by smooth lines.

TABLE 2. X-ray Standing Wave Results for U(VI) Sorbed to Calcite (104) Cleavage Surfaces

$[^{236}U]_{aq}$ (mol/L)	$P_{(104)}$	$f_{(104)}$	Θ_{Tot} (monolayer)	Θ_{Coh} (monolayer)
5.0×10^{-5}	0.83 ± 0.02	0.50 ± 0.04	0.06	0.03
5.0×10^{-5}	0.86 ± 0.02	0.62 ± 0.07	0.05	0.03
9.8×10^{-5}	0.86 ± 0.02	0.15 ± 0.04	0.43	0.06
9.8×10^{-5}	0.83 ± 0.02	0.44 ± 0.04	0.35	0.15
1.3×10^{-4}	0.80 ± 0.02	0.37 ± 0.04	n.d.	n.d.

powders showing the influence of the SA/V ratio on coverage at fixed U(VI) concentration (Figure 3) can be extrapolated to higher coverage as SA/V approaches zero. The enhanced surface roughening in response to the EDTA in the most concentrated solutions, as evidenced in the AFM images (Figure 1), may also cause an increase of U(VI) sorption for the higher U(VI) solution concentrations, consistent with the observed deviation in coverage between the powder and single-crystal sorption measurements.

XSW Measurements. Five measurements of sorbed U(VI) on calcite (104) surfaces were performed with XSW generated by Bragg reflection from the H=(104) lattice plane. An XSW scan for a typical sample is shown in Figure 5, along with the best-fit curve based on eq 2. Results for the five measurements are summarized in Table 2. The measured coherent position, P_H, ranges from 0.80 to 0.86, has a mean value of 0.84 ± 0.02, and is independent of the solution composition within the range of experimental conditions. The coherent fraction, f_H, ranges from 0.15 to 0.62, and the total U coverage Θ_{tot} ranges from 0.05 to 0.43 monolayers. The coherent coverage Θ_{Coh} is calculated from the total coverage as follows:

$$\Theta_{Coh} = f_{(1014)} \times \Theta_{tot} \quad (3)$$

Therefore, Θ_{Coh} ranges from 0.03 to 0.15 monolayers.

The relatively high values of the coherent fraction for U indicate that the U is located mostly in a specific crystallographic plane above the calcite (104) surface. If the U were either randomly distributed or concentrated in separate,

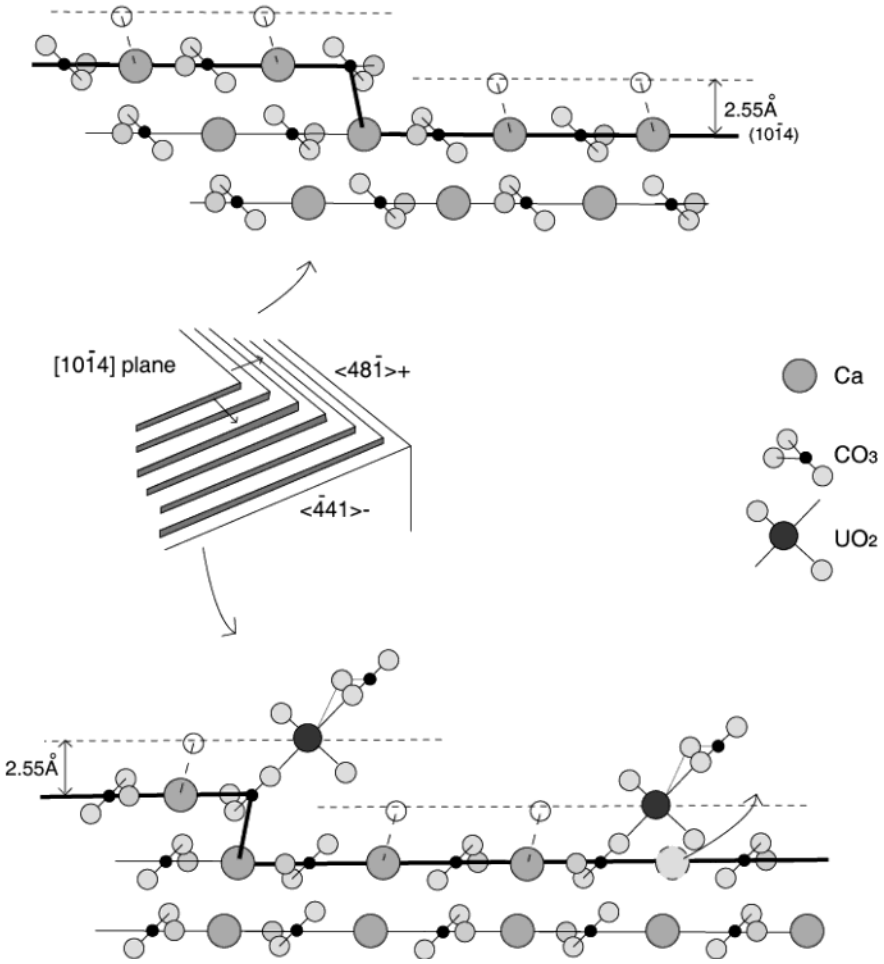

FIGURE 6. Ball-and-stick representation of postulated uranyl−carbonate surface complexes on calcite. Geometries of the two nonequivalent steps developed along the ⟨48$\bar{1}$⟩ and the ⟨$\bar{4}$41⟩ directions during calcite dissolution are shown (*68*). The proposed geometries of U(VI) ternary carbonato-complexes involving single CO_3 groups at either the labeled "−" step sites or the equivalent terrace defect sites are represented. For clarity, the third CO_3 group bound to U(VI) is omitted. To illustrate the slight rotation of the uranyl unit away from the plane of the page, lengths of the two U−O_{ax} bonds are nonequal. Also shown are oxygens (representing water molecules) bound to surface Ca ions at 2.50 ± 0.12 Å above the (104) plane, from X-ray reflectivity results of ref *69*.

U-rich phases, an apparent random distribution would be indicated by $f_H \sim 0$ in the XSW data which is not the observed case. However, because the coherent fraction is significantly less than unity, at least some of the U(VI) may occur in a position other than that specified by the coherent position. This "incoherent" fraction could be other U(VI) species adsorbed to the surface or incorporated within the surface. However, when the coherent fraction equals or exceeds a value of about 0.4, the U is located mostly in a single plane as defined by the coherent position (*50*).

From the mean coherent position of U, the projected height h_H of the U atoms in the [104] direction can be derived using the following relation: $h_H = P_H \times d_H$, where d_H is the lattice spacing of the (104) diffraction plane (= 3.04 Å in this case). The mean h_H value for U(VI) normal to the (104) lattice plane is therefore 2.55 ± 0.06 Å. Although the modulo-d ambiguity of the X-ray standing wave method allows the position of the U to be integral d_H values away from this position, such as 2.55 + 3.04 Å = 5.59 Å above the surface (104) plane, it appears more likely that the uranyl is bound to the surface in an inner-sphere configuration. We cannot envision an inner-sphere coordination that would result in a distance greater than about 3.2 Å between the U(VI) and the surface (104) plane. Other configurations involving greater distances, such as an outer-sphere configuration with water molecules between the U(VI) and the calcite (104) plane, would be unlikely to yield the observed high values of f_H because of the relatively high disorder of U(VI) in such configurations.

Discussion

The XSW measurements indicate that the U(VI) is sorbed at one (or more) fairly well constrained crystallographic site(s) at the calcite (104) surface under the conditions that we investigated. If the U(VI) occupies multiple sites, then these sites must occur mostly within a single plane parallel to calcite (104) in order to satisfy the constraints of the XSW data. The significant deviation of the U coherent position from the Ca coherent position indicates that simple substitution of U(VI) for Ca^{2+} at the calcite (104) surface does not explain the results. Rather, sorption is best explained by surface complexation of a uranyl−carbonate species via inner-sphere bonding of U with a surface carbonate group. Elzinga et al. (*30*) reached the same conclusion independently from EXAFS and luminescence spectroscopy data.

The possible geometries of uranyl−carbonate surface complexes that meet the constraints of the XSW data as well as the steric constraints of the calcite (104) surface structure are shown schematically in Figure 6. A key constraint on the U(VI) atom location is the 2.34 to 2.43 Å U−O_{eq} distance that is typically observed for five- or six-coordinated U(VI), respectively, in crystal structures (*70*). Monodentate coordination of sorbed U(VI) with O_{surf} atoms is clearly feasible

because U−O_{surf} distances within this 2.34−2.43 Å range can be obtained, with a 2.55 Å distance between the U atom and the surface (104) plane, by involving only a minor relaxation of the surface carbonate group. Such relaxations of surface carbonate groups accompanying incorporation of metal ion impurities at the calcite (104) surface (e.g., refs *54* and *55*) and within bulk calcite (*33*, *34*, *57*, *71*) are well documented. Bidentate coordination of the sorbed U(VI) with a surface carbonate group is also possible but requires a larger amount of relaxation of the surface carbonate than does monodentate coordination; at least two of the carbonate O atoms must lie above the surface (104) plane to accommodate the 2.55 Å distance between it and the U(VI) atom while maintaining the requisite 2.43 Å bidentate U−O_{eq} distance.

Steric constraints dictate that U(VI) surface complexes on calcite can form preferentially at the $\langle\bar{4}41\rangle$_ and $\langle 48\bar{1}\rangle$_ (or "−") step sites, whereas at the "+" step sites the lower O_{ax} of the uranyl ion impinges on the calcite surface. This conclusion is consistent with the results of Reeder et al. (*29*), who showed that U(VI) is differentially incorporated between nonequivalent vicinal faces of a growth hillock, reflecting step-selective incorporation of uranyl species at the $\langle\bar{4}41\rangle$_ and $\langle 48\bar{1}\rangle$_ steps. Moreover, this configuration is supported by bond-strength calculations (*72*). Using bond-valence parameters for uranyl coordination with five equatorial oxygens (*70*), the expected bond strength of the U−O_{eq} link is about 0.5 valence units, assuming a mean U−O_{eq} distance of 2.35 Å. The protruding O_{surf} atoms from the CO_3 groups at the $\langle\bar{4}41\rangle$_ and $\langle 48\bar{1}\rangle$_ steps display a vacant charge approaching 0.66^- valence units, significantly more negative than other O_{surf} atoms. Preferential formation of U(VI)-O_{surf} bonds at the "−" steps is thus favored to achieve local charge balance, and attachment of a uranyl−carbonate surface complex at that site is allowed by its open geometry.

Although we have established that the proposed uranyl−carbonate surface complex may form at "−" steps, we note that the step density estimated from the AFM image of EDTA-reacted calcite (Figure 1b) is apparently too low to account for the amount of sorbed U(VI). For example, if the estimated step density (792 m/cm^2, estimated from Figure 1b) was saturated with sorbed U(VI) at one U atom every 4 Å, then the maximum surface coverage would be 0.004 monolayers. Because the steps are probably not saturated with U(VI) and the step density on calcite reacted under higher surface area/volume conditions is lower than that portrayed in Figure 1b, the probable surface coverage of U(VI) that can be accommodated by surface complexation at steps is lower than 0.004 monolayers. The data of Carroll and Bruno (*26*) imply that U(VI) adsorption probably takes place on terrace areas given the high surface coverages (∼0.05 to ∼0.7) measured in that study. Thus, a second, "unlimited" site may be inferred, as suggested by the linearity of the Freundlich sorption isotherm over 4 orders of magnitude range in solution U(VI) concentration (Figure 4). Therefore, it seems that complexation with O_{surf} atoms on terraces must be involved to account for the measured high U(VI) coverages. Because of the steric constraints discussed above, the only way to accommodate a uranyl surface complex on a calcite (104) terrace is adjacent to a Ca vacancy or small etch pit, effectively equivalent to a short "−" step site (Figure 6). If much of the sorbed U(VI) occurs as surface complexes adjacent to Ca vacancies, this could imply the release of one Ca^{2+} ion for each U(VI) sorbed atom on a terrace area. This process would result in an apparent linear relationship between the concentration of dissolved U(VI) and the amount of dissolved Ca^{2+}, which could be interpreted within a thermodynamic context as a surface exchange reaction between UO_2^{2+} and Ca^{2+} (*26*, *32*).

Although we cannot uniquely identify the surface uranyl species from XSW data, the fact that the dominant aqueous uranyl species predicted to be present under the conditions of the experiments is $Ca_2UO_2(CO_3)_3^0$ indicates possible involvement of this species in the adsorption mechanism. This conclusion is in excellent agreement with another recent study of uranyl adsorption on calcite at pH 7.4 and 8.3 and PCO_2 of $10^{-3.5}$ atm (*30*), where a uranyl−triscarbonate inner-sphere surface complex identified by a combination of EXAFS and luminescence spectroscopy appeared to be the dominant sorption species at solution U(VI) concentration <500 μM. The solution speciation of U(VI) was dominated by uranyl−triscarbonate species in our experiments as well as those of ref *30*. Ternary uranyl−carbonate surface complexes have been identified also in a number of studies of uranyl sorption on amorphous and crystalline Fe-oxides and -oxyhydroxides (*4*, *6*, *8*, *14*, *16*, *17*, *73*). Although uranyl−carbonate species are stable in aqueous solution, they are also commonly adsorbed to mineral surfaces.

A final question that may be asked is how sorbed U(VI) may be incorporated within bulk calcite during crystal growth (*28*, *29*). This is envisioned with reference to Figure 6. The equatorial plane of the sorbed uranyl complex could rotate to become parallel to the (104) plane, if the lower O_{ax} atom displaces a carbonate ion in the underlying calcite (104) surface. Then calcite could precipitate around the uranyl, provided another carbonate ion is displaced by the upper O_{ax} atom in the (104) plane overlying the U(VI) atom. Uranyl incorporated in this way effectively substitutes for a Ca ion and is consistent with the model for trace uranyl incorporation in bulk calcite based on the EXAFS data of ref *34*.

Acknowledgments

Work supported by the Geosciences Research Program of the U.S. Department of Energy's Office of Basic Energy Sciences. The Advanced Photon Source is supported by the U.S. Department of Energy, Office of Science, Office of Basic Energy Sciences under Contract W-31-109-Eng-38. A Lavoisier Fellowship from the French Ministry of Foreign Affairs supported the postdoctoral research of S. Rihs at Argonne National Laboratory. The authors acknowledge the efforts of *ES&T* Associate Editor Janet G. Hering as well as R. J. Reeder and two anonymous reviewers who provided constructive comments on the manuscript.

Literature Cited

(1) Langmuir, D. Uranium solution-mineral equilibria at low temperature with applications to sedimentary ore deposits. *Geochim. Cosmochim. Acta* **1978**, *42*, 547−569.

(2) Grenthe, I.; Fuger, J.; Konings, R.; Lemire, R. J.; Muller, A. B.; Nguyen-Trung, C.; Wanner, J. *Chemical Thermodynamics of Uranium*; North-Holland, Amsterdam, 1992.

(3) Tsunashima, A.; Brindley, G. W.; Bastovanov, M. Adsorption of uranium from solutions by montmorillonite: compositions and properties of uranyl montmorillonites. *Clays Clay Miner.* **1981**, *29*, 10−16.

(4) Hsi, C. K. D.; Langmuir, D. Adsorption of uranyl onto ferric oxyhydroxides: Application of the surface complexation site-binding model. *Geochim. Cosmochim. Acta* **1985**, *49*, 1931−1941.

(5) Dent, A. J.; Ramsay, J. D.; Swanton, S. W. An EXAFS study of uranyl ion in solution and sorbed onto silica and montmorillonite clay colloids. *J. Colloid Interface Sci.* **1992**, *150*, 45−60.

(6) Waite, T. D.; Payne, T. E.; Davis, J. A.; Sekine, K. *Uranium sorption: Alligator rivers analogue project*; Final report, No. 13; Australian Nucl. Sci. Technol. Org., 1992.

(7) Chisholm-Brause, C.; Conradson, S. D.; Buscher, C. T.; Eller, P. G.; Morris, D. Speciation of urnayl sorbed at multiple binding sites on montmorillonite. *Geochim. Cosmochim. Acta* **1994**, *58*, 3625−3631.

(8) Waite, T. D.; Davis, J. A.; Payne, T. E.; Waychunas, G. A.; Xu, N. Uranium(VI) adsorption to ferrihydrite: Application of a surface complexation model. *Geochim. Cosmochim. Acta* **1994**, *58*, 5465−5478.

(9) Bruno, J.; De Pablo, J.; Duro, L.; Figuerola, E. Experimental study and modeling of the U (VI)-Fe(OH)$_3$ surface precipitation/coprecipitation equilibria. *Geochim. Cosmochim. Acta* **1995**, *59*, 4113−4123.
(10) McKinley, J. P.; Zachara, J. M.; Smith, S. C.; Turner, D. R. The influence of hydrolysis and multiple site-binding reactions on adsorption of U(VI) to montmorillonite. *Clays Clay Miner.* **1995**, *43*, 586−598.
(11) Duff, M. C.; Amrhein, C. Uranium (VI) adsorption on goethite and soil in carbonate solutions. *Soil Sci. Soc. Am. J.* **1996**, *60*, 1393−1400.
(12) Turner, D. R.; Zachara, J. M.; McKinley, J. P.; Smith, S. C. Surface-charge properties and UO_2^{2+} adsorption of a subsurface smectite. *Geochim. Cosmochim. Acta* **1996**, *60*, 3399−3414.
(13) Pabalan, R. T.; Turner, D. R.; Bertetti, F. P.; Prikryl, J. D. Uranium VI sorption onto selected mineral surfaces: key geochemical parameters. In *Adsorption of Metals by Geomedia*; Jenne, E. A., Ed.; Academic Press: New York, 1998; pp 99−130.
(14) Reich, T.; Moll, H.; Arnold, T.; Denecke, M. A.; Henning, C.; Geipel, G.; Bernhard, G.; Nitsche, H.; Allen, P. G.; Bucher, J. J.; Edelstein, N. M.; Shuh, D. K. An EXAFS study of uranium (VI) sorption onto silica gel and ferrihydrite. *J. Electron Spectrosc. Relat. Phenom.* **1998**, *96*, 237−243.
(15) Allard, T.; Ildefonse, P.; Beaucaire, C.; Calas, G. Structural chemistry of uranium associated with Si, Al, Fe gels in a granitic uranium mine. *Chem. Geol.* **1999**, *158*, 81−103.
(16) Bargar, J. R.; Reitmeyer, R.; Davis, J. A. Spectroscopic confirmation of uranium(VI)-carbonato adsorption complexes on hematite. *Environ. Sci. Technol.* **1999**, *33*, 2481−2484.
(17) Bargar, J. R.; Reitmeyer, R.; Lenhart, J. J.; Davis, J. A. Characterization of U(VI)-carbonato ternary complexes on hematite: EXAFS and electrophoretic mobility measurements. *Geochim. Cosmochim. Acta* **2000**, *64*, 2737−2749.
(18) Sylwester, E. R.; Hudson, E. A.; Allen, P. G. The stucture of uranium (VI) sorption complexes on silica, alumina and montmorillonite. *Geochim. Cosmochim. Acta* **2000**, *64*, 2431−2438.
(19) Chisholm-Brause, C.; Berg, J. M.; Matzner, R. A.; Morris, D. Uranium(VI) sorption complexes on montmorillonite as a function of solution chemistry. *J. Colloid Interface Sci.* **2001**, *233*, 38−49.
(20) Giammar, D. Geochemistry of uranium at mineral-water interfaces: rates of sorption−desorption and dissolution-precipitation reactions. Ph.D. Thesis, California Institute of Technology, 2001.
(21) Prikryl, J. D.; Jain, A.; Turner, D. R.; Pabalan, R. T. Uranium^{VI} sorption behavior on silicate mineral mixtures. *J. Contam. Hydrol.* **2001**, *47*, 241−253.
(22) Froideval, A.; Del Nero, M.; Barillon, R.; Hommet, J.; Mignot, G. pH dependence of uranyl retention in a quartz/solution system: an XPS study. *J. Colloid Interface Sci.* **2003**, *266*, 221−235.
(23) Rihs, S.; Condomines, M.; Sigmarsson, O. U, Ra and Ba incorporation during precipitation of hydrothermal carbonates: implications for ^{226}Ra−Ba dating of impure travertines. *Geochim. Cosmochim. Acta* **2000**, *64*, 661−671.
(24) Morse, J. W.; Shanbhag, P. M.; Saito, A.; Choppin, G. R. Interaction of uranyl ions in carbonate media. *Chem. Geol.* **1984**, *42*, 85−99.
(25) Milton, G.; Brown, R. Adsorption of uranium from groundwater by common fracture secondary minerals. *Can. J. Earth Sci.* **1987**, *24*, 1321−1328.
(26) Carroll, S. A.; Bruno, J. Mineral-solution interactions in the U(VI)-CO_2−H_2O system. *Radiochim. Acta* **1991**, *52/53*, 187−193.
(27) Meece, D. E.; Benninger, L. K. The coprecipitation of Pu and other radionuclides with $CaCO_3$. *Geochim. Cosmochim. Acta* **1993**, *57*, 1447−1458.
(28) Reeder, R. J.; Nugent, M.; Lamble, G. M.; Tait, C. D.; Morris, D. E. Uranyl incorporation into calcite and aragonite: XAFS and luminescence studies. *Environ. Sci. Technol.* **2000**, *34*, 638−644.
(29) Reeder, R. J.; Nugent, M.; Tait, C. D.; Morris, D. E.; Heald, S. M.; Beck, K. M.; Hess, W. P.; Lanzirotti, A. Coprecipitation of uranium(VI) with calcite: XAFS, micro-XAS, and luminescence characterization. *Geochim. Cosmochim. Acta* **2001**, *65*, 3491−3503.
(30) Elzinga, E. J.; Tait, C. D.; Reeder, R. J.; Rector, K. D.; Donohoe, R. J.; Morris, D. E. Spectroscopic investigation of U(VI) sorption at the calcite-water interface. *Geochim. Cosmochim. Acta* **2004**, *68*, 2437−2448.
(31) *Uranium-series disequilibrium*; Ivanovich, M., Harmon, R. S., Eds.; Oxford: Oxford, 1992.
(32) Geipel, G.; Reich, T.; Brendler, V.; Bernhard, G.; Nitsche, H. Laser and X-ray spectroscopic studies of uranium-calcite interface phenomena. *J. Nuclear Mater.* **1997**, *248*, 408−411.
(33) Sturchio, N. C.; Antonio, M. R.; Soderholm, L. B.; Sutton, S. R.; Brannon, J. C. Tetravalent uranium in calcite. *Science* **1998**, *281*, 971−973.
(34) Kelly, S. D.; Newville, M. G.; Cheng, L.; Kemner, K. M.; Sutton, S. R.; Fenter, P.; Sturchio, N. C.; Spötl, C. Uranyl incorporation in natural calcite. *Environ. Sci. Technol.* **2003**, *37*, 1284−1287.
(35) Toste, A. P.; Lechner-Fish, T. J. Organic diagenesis in commercial, low-level nuclear wastes. *Radioact. Waste Manage. Nucl. Fuel Cycle* **1989**, *12*, 291−301.
(36) Riley, R. G.; Zachara, J. M. Chemical contaminants on DOE lands and selection of contaminant mixtures for subsurface science research. U.S. Government Printing Office: Washington, DC, 1992; DOE/ER-0547T.
(37) Read, D.; Ross, D.; Sims, R. J. The migration of uranium through Clashach sandstone: the role of low molecular weight organics in enhancing radionuclide transport. *J. Contam. Hydrol.* **1998**, *35*, 235−248.
(38) Gephart, R. E.; Lundgren, R. E. *Hanford Tank Cleanup: A Guide to Understanding the Technical Issues;* Battelle Memorial Institute: Columbus, OH, 1998.
(39) Morel, F. M. M.; Hering, J. G. *Principles and applications of aquatic chemistry*; Wiley-Interscience: New York, 1993.
(40) Means, J. L.; Crerar, D. A.; Duguid, J. O. Migration of radioactive wastes: radionuclide mobilization by complexing agents. *Science* **1978**, *200*, 1477−1481.
(41) Cross, J. E.; Ewart, F. T.; Greenfield, B. F. Modelling the behaviour of organic degradation products. *Mater. Res. Soc. Symp. Proc.* **1989**, *127*, 715.
(42) Allison, J. D.; Brown, D. S.; Novo-Gradac, N. K. *MINTEQA2: a geochemical assessment model for environmental systems*, U.S. EPA: Athens, Georgia, 1991; Report No. 600/3-91/021.
(43) Silva, R. J. Mechanisms for the retardation of uranium(VI) migration. *Mater. Res. Soc. Symp. Proc.* **1992**, *257*, 323−330.
(44) Sandino, A.; Bruno, J. The solubility of $(UO_2)_3(PO_4)_2{\cdot}4H_2O$(s) and the formation of U(VI) phosphate complexes: their influence in uranium speciation in natural waters. *Geochim. Cosmochim. Acta* **1992**, *56*, 4135−4145.
(45) Smith, R. M.; Martell, A. E. In *Critical stability constants (revised). Vol. 6, Second Supplement*; Plenum Press: New York, 1989; pp 96−99.
(46) Bernhard, G.; Geipel, G.; Reich, T.; Brendler, V.; Amayri, S.; Nitsche, H. Speciation of uranium in seepage waters of a mine tailing pile studied by time-resolved laser-induced fluorescence spectroscopy (TRLFS). *Radiochim. Acta* **2001**, *89*, 511−518.
(47) Torrero, M. E.; Casas, I.; De Pablo, J.; Sandino, M.; Grambow, B. A Comparison between unirradiated UO_2(s) and Schoepite solubilities in 1M NaCl Medium. *Radiochim. Acta* **1994**, *66/67*, 29−35.
(48) Jacquier, P.; Meier, P.; Ly, J. Adsorption of radioelements on mixture of minerals − experimental study. *Appl. Geochem.* **2001**, *16*, 85−93.
(49) Lee, Y. J.; Morse, J.; Wiltschko, V. An experimentally verified model for calcite precipitation in veins. *Chem. Geol.* **1996**, *130*, 203−215.
(50) Bedzyk, M. J.; Cheng, L. X-ray standing wave studies of minerals and mineral surfaces: principles and applications. *Rev. Mineral. Geochem.* **2002**, *49*, 221−266.
(51) Qian, Y. L.; Sturchio, N. C.; Chiarello, R. P.; Lyman, P. F.; Lee, T. L.; Bedzyk, M. J. Lattice location of trace elements within minerals and at their surfaces with X-ray standing waves. *Science* **1994**, *265*, 1555−1557.
(52) Sturchio, N. C.; Chiarello, R. P.; Cheng, L.; Lyman, P. F.; Bedzyk, M. J.; Qian, Y.; You, H.; Yee, D.; Geissbühler, P.; Sorensen, L.; Liang, Y.; Baer, D. Lead adsorption at the calcite-water interface: Synchrotron X-ray standing wave and X-ray reflectivity studies. *Geochim. Cosmochim. Acta* **1997**, *61*, 251−263.
(53) Cheng, L.; Lyman, P.; Sturchio, N. C.; Bedzyk, M. J. Adsorption and structure of selenite anions on the calcite (104) surface. *Surf. Sci.* **1997**, *382*, 690−695.
(54) Cheng, L.; Sturchio, N. C.; Woicik, J. C.; Kemner, K. M.; Lyman, P.; Bedzyk, M. J. High-resolution structural study of zinc ion incorporation at the calcite cleavage surface. *Surf. Sci.* **1998**, *415*, 976−982.
(55) Cheng, L.; Fenter, P.; Sturchio, N. C.; Zhong, Z.; Bedzyk, M. J. X-ray standing wave study of arsenite incorporation at the calcite surface. *Geochim. Cosmochim. Acta* **1999**, *63*, 3153−3157.
(56) Cheng, L.; Sturchio, N. C.; Bedzyk, M. J. Local structure of Co(II) incorporated at the calcite surface: An XSW and SEXAFS study. *Phys. Rev. B* **2000**, *61*, 4877−4883.

(57) Cheng, L.; Sturchio, N. C.; Bedzyk, M. J. Impurity structure in a molecular ionic crystal: Atomic-scale X-ray study of $CaCO_3$: Mn^{2+}. *Phys. Rev. B* **2001**, *63*, 144104: 1−7.
(58) Fenter, P.; Cheng, L.; Rihs, S.; Machesky, M.; Bedzyk, M. J.; Sturchio, N. C. Electrical double-layer structure at the rutile-water interface as observed in situ with small-period X-ray standing waves. *J. Colloid Interface Sci.* **2000**, *225*, 154−165.
(59) Dreybrodt, W.; Lauckner, J.; Zaihua, L.; Svensson, U.; Buhmann, D. The kinetics of the reaction $CO_2 + H_2O \rightarrow H^+ + HCO_3^-$ as one of the rate-limiting steps for the dissolution of calcite in the system $H_2O-CO_2-CaCO_3$. *Geochim. Cosmochim. Acta* **1996**, *60*, 3375−3381.
(60) Fredd, C. N.; Fogler, H. S. The influence of chelating agents on the kinetics of calcite dissolution. *J. Colloid Interface Sci.* **1998**, *204*, 187−197.
(61) Friis, A. K.; Davis, T. A.; Figueira, M. M.; Paquette, J.; Mucci, A. Influence of *Bacillus subtilis* cell walls and EDTA on calcite dissolution rates and crystal surface features. *Environ. Sci. Technol.* **2003**, *37*, 2376−2382.
(62) Davis, J.; Fuller, C.; Cook, A. A model for trace metal sorption processes at the calcite surface: adsorption of Cd^{2+} and subsequent solid solution formation. *Geochim. Cosmochim. Acta* **1987**, *51*, 1477−1490.
(63) Giammar, D.; Hering, J. G. Time scales for sorption−desorption and surface precipitation of uranyl on goethite. *Environ. Sci. Technol.* **2001**, *35*, 3332−3337.
(64) Sparks, D. L. Kinetics and mechanisms of chemical reactions at the soil mineral/water interface. In *Soil physical chemistry*; Sparks, D. L., Ed.; CRC Press: 1999.
(65) Barrow, N. J.; Gerth, J.; Brümmer, G. W. Reaction kinetics of the adsorption and desorption of nickel, zinc and cadmium by goethite. II. Modelling the extent and rate of reaction. *J. Soil Sci.* **1989**, *40*, 437−450.
(66) Brümmer, G. W.; Gerth, J.; Tiller, K. G. Reaction kinetics of the adsorption and desorption of nickel, zinc and cadmium by goethite. I. Adsorption and diffusion of metals. *J. Soil Sci.* **1988**, *39*, 23−28.
(67) Scheinost, A. C.; Abend, S.; Pandya, K. I.; Sparks, D. L. Kinetic controls on Cu and Pb sorption by ferrihydrite. *Environ. Sci. Technol.* **2001**, *35*, 1090−1096.
(68) Liang, Y.; Baer, D. R. Anisotropic dissolution at the $CaCO_3$ $(10\bar{1}4)$−water interface. *Surf. Sci.* **1997**, *373*, 275−287.
(69) Fenter, P.; Geissbühler, P.; Di Masi, E.; Srajer, G.; Sorensen, L.; Sturchio, N. C. Surface speciation of calcite observed in situ with X-ray scattering. *Geochim. Cosmochim. Acta* **2000**, *64*, 1221−1228.
(70) Burns, P. C.; Ewing, R. C.; Hawthorne, F. C. The crystal chemistry of hexavalent uranium: polyhedral geometries, bond-valence parameters, and polymerization of polyhedra. *Can. Mineral.* **1997**, *35*, 1551−1570.
(71) Reeder, R. J.; Lamble, G. M.; Northrup, P. A. XAFS study of the coordination and local relaxation around Co^{2+}, Zn^{2+}, Pb^{2+} and Ba^{2+} trace elements in calcite. *Am. Mineral.* **1999**, *84*, 1049−1060.
(72) Brown, I. D. The bond-valence method: an empirical approach to chemical structure and bonding. In *Structure and bonding in crystals II*; O'Keeffe, M., Navrotsky, A., Eds.; Academic Press: New York, 1981; pp 1−30.
(73) Ho, C. H.; Miller, N. H. Adsorption of uranyl species from bicarbonate solution onto hematite particles. *J. Colloid Interface Sci.* **1986**, *110*, 165−171.

Received for review January 29, 2004. Revised manuscript received July 23, 2004. Accepted July 26, 2004.

ES049847B